ARTICLES
PUBLISHED ONLINE: 19 FEBRUARY 2012 | DOI: 10.1038/NMAT3250
nature materials

Controlling the Curie temperature in (Ga,Mn)As through location of the Fermi level within the impurity band

M. Dobrowolska[1]*, K. Tivakornsasithorn[1], X. Liu[1], J. K. Furdyna[1], M. Berciu[2], K. M. Yu[3] and W. Walukiewicz[3]

The ferromagnetic semiconductor (Ga,Mn)As has emerged as the most studied material for prototype applications in semiconductor spintronics. Because ferromagnetism in (Ga,Mn)As is hole-mediated, the nature of the hole states has direct and crucial bearing on its Curie temperature T_C. It is vigorously debated, however, whether holes in (Ga,Mn)As reside in the valence band or in an impurity band. Here we combine results of channelling experiments, which measure the concentrations both of Mn ions and of holes relevant to the ferromagnetic order, with magnetization, transport, and magneto-optical data to address this issue. Taken together, these measurements provide strong evidence that it is the location of the Fermi level within the impurity band that determines T_C through determining the degree of hole localization. This finding differs drastically from the often accepted view that T_C is controlled by valence band holes, thus opening new avenues for achieving higher values of T_C.

Understanding the factors that control the Curie temperature T_C in (Ga,Mn)As is of obvious importance, as it can serve as a guide for strategies to optimize this material. This issue is closely linked to the question of whether the holes mediating the Mn–Mn interaction reside in a weakly disordered valence band, or in an impurity band. Despite extensive studies, this question is still vigorously debated[1]. The valence band model assumes that a separated impurity band does not exist for Mn concentrations higher than ~1–2% (refs 2,3), and successfully accounts for a number of observations[2–12]. The alternative model assumes that the holes reside in a Mn-derived impurity band even for moderate to high Mn concentrations[13–15], and there is also a wealth of experimental papers favouring this picture[16–26].

When Mn ions substitute for Ga in (Ga,Mn)As, they become acceptors, introducing holes that mediate ferromagnetic interactions between the $S = 5/2$ moments of the half-filled $3d$ Mn shells. However, as was described theoretically[16] and observed experimentally[27], during (Ga,Mn)As growth some of the Mn ions also enter into interstitial sites (Mn_I), becoming highly mobile positively charged double donors. They can, however, be immobilized by Coulomb attraction at interstitial sites immediately adjacent to the negatively charged Mn_{Ga}, where they form antiferromagnetically coupled Mn_I–Mn_{Ga} pairs, as was shown both theoretically[28,29] and experimentally[30–32]. This automatically lowers the fraction of Mn contributing to ferromagnetic order to $x_{eff} = x_{sub} - x_I$, where x_{sub} and x_I are respectively the concentrations of Mn_{Ga} and Mn_I. As Mn_I are double donors, they also reduce the concentration of the holes by compensation to $p = 4(x_{sub} - 2x_I)/a^3$, where a is the lattice constant of (Ga,Mn)As.

The early mean-field theory, based on the assumption that holes reside in the valence band, predicts[2] that $T_C \sim x_{eff}\, p^{1/3}$. Later this theory was expanded by Jungwirth *et al.*[33] to include further refinements, such as discreteness of random Mn_{Ga} positions in the lattice and antiferromagnetic superexchange contributions to the near-neighbour Mn_{Ga}–Mn_{Ga} coupling. The general prediction of this more advanced formulation of the valence band model is that T_C increases monotonically with x_{eff} and p. As in both theories the two key parameters are p and x_{eff}, their experimental verification is hindered by the fact that accurate determination of the total hole concentration, especially in insulating samples, is quite difficult if one uses electrical measurements, because this contains little if any contribution from localized holes; and the anomalous Hall effect in ferromagnetic (Ga,Mn)As adds an extra level of complication. Furthermore, the value of x_{eff} is usually determined from magnetization data, and this determination is based on an assumed value of magnetic moment per x_{eff}, which is not fully known.

In this paper we take a direct approach for determining both the effective Mn concentration x_{eff} and the hole concentration p from one experiment, namely, we map out the location of Mn in the lattice by simultaneously using channelling Rutherford backscattering (c-RBS) and channelling particle-induced X-ray emission (c-PIXE), which automatically yield the concentration of Mn_{Ga} (x_{sub}) and Mn_I (x_I), allowing us to directly evaluate x_{eff} and p. These measurements were performed on a series of ten samples, both as-grown and annealed, with a total Mn concentration x_{tot} ranging between 0.03 and 0.068, encompassing a wide range of samples having different degrees of compensation and transport behaviours that vary from insulating to metallic. We also performed transport, magnetization and magnetic circular dichroism (MCD) measurements on the same samples. This is the first time that such a detailed and systematic study of the location of Mn ions in the lattice and its correlation with other experiments has been carried out. Taken together, our

[1]Department of Physics, University of Notre Dame, Notre Dame, Indiana 46556, USA, [2]Department of Physics and Astronomy, University of British Columbia, Vancouver, British Columbia V6T 1Z1, Canada, [3]Materials Science Division, Lawrence Berkeley National Laboratory, Berkeley, California, 94720, USA. *e-mail: mdobrowo@nd.edu.

Table 1 | Local structure of (Ga,Mn)As as determined by channelling experiments.

Sample	x_{tot} (%)	x_{random} (%)	x_{sub} (%)	x_I (%)	x_{eff} (%)	T_C (K)	p (10^{20} cm^3)	p/N_{Mn}^{eff} or f
A (as grown)	3.0	0.1	2.4	0.5	1.9	45	3.1	0.74
B (as grown)	3.5	0.1	3.2	0.2	3.0	27	6.2	0.93
C (as grown)	4.8	0.3	4.0	0.5	3.5	34	6.6	0.86
C* (annealed)	5.0	0.4	4.3	0.3	4.0	54	8.2	0.93
D (as grown)	5.8	0.3	5.0	0.5	4.5	26	8.8	0.90
D* (annealed)	5.9	0.4	5.3	0.2	5.1	42	10.8	0.96
E (as grown)	6.0	0.3	5.0	0.7	4.3	30	8.0	0.84
E* (annealed)	6.1	0.5	5.2	0.4	4.8	43	9.7	0.92
F (as grown)	6.4	0.5	4.2	1.7	2.5	40	1.8	0.32
F* (annealed)	6.8	1.3	4.5	1.0	3.5	90	5.5	0.71

The location of Mn sites in the lattice was determined by simultaneous c-PIXE and c-RBS. Here x_{tot} indicates the total Mn concentration; x_{random} the concentration of Mn atoms residing at random locations, for example, MnAs inclusions; x_{sub} the concentration of Mn ions located at Ga lattice sites (Mn_{Ga}); and x_I the concentration of Mn ions located at interstitial sites (Mn_I). The quantity $x_{eff} = x_{sub} - x_I$ is the concentration of Mn ions which contributes to ferromagnetic order. The hole concentration p for a given sample was found as $p = 4(x_{sub} - 2x_I)/a^3$, where a is the lattice constant of (Ga,Mn)As of that sample calculated according to ref. 38. The Curie temperature T_C is determined from magnetization measurements versus temperature. Finally, p/N_{Mn}^{eff} is the number of holes per effective Mn moment $N_{Mn}^{eff} = 4(x_{eff})/a^3$. It is easily seen that p/N_{Mn}^{eff} is equal to the filling factor of the impurity band $f = (x_{sub} - 2x_I)/x_{eff}$ used later in discussing the location of the Fermi level. Even though there is a general tendency for x_I/x to increase in samples with higher Mn concentration, in practice its value is a very sensitive function of growth conditions, that is, the probability for Mn_I to form depends on both the Mn flux and the growth temperature.

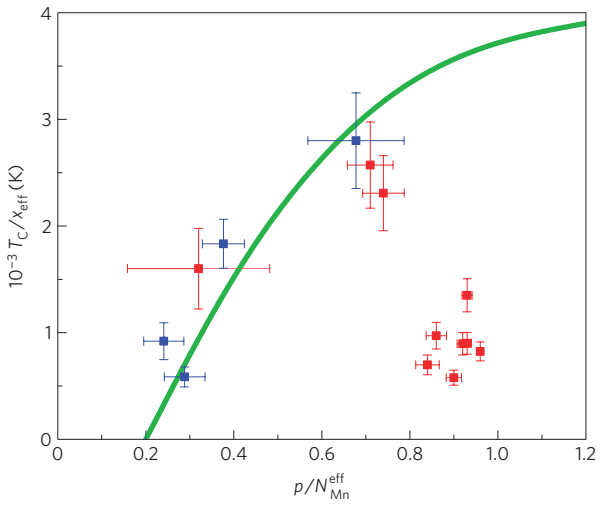

Figure 1 | Comparison between experimental data and theoretical calculations based on the valence band model of Jungwirth *et al.*[33]. The calculations according to ref. 33 (green curve) were carried out within the TBA/CPA model based on the valence band picture, and include such effects as hole–hole exchange interaction, discreteness of random Mn_{Ga} position in the lattice, and other refinements. The calculations and the data shown in the figure are plotted as T_C/x_{eff} versus p/N_{Mn}^{eff} (where p/N_{Mn}^{eff} is the ratio of the hole concentration to the concentration of effective Mn moments N_{Mn}^{eff}, with $N_{Mn}^{eff} = 4x_{eff}/a^3$). The theoretical calculations of ref. 33 predict that for high compensation the Curie temperature falls with decreasing hole concentration. In the low-compensation regime, however, these predictions show that T_C is almost independent of the hole density. The experimental data shown in the figure are taken from Table 1 (red squares) and from ref. 40 (blue squares). For samples in the low-compensation range the experimental points are seen to depart drastically from the theoretical predictions of the valence band model. The error bars in the figure are calculated using standard analysis of error propagation, that is, $\delta f^2 = \sum_i^n (\partial f/\partial x_i)^2 (\delta x_i)^2$, where the error bars are given by δf, and δx_i are the standard deviations of Mn_I, Mn_{Ga} and T_C.

results challenge the valence band picture of ferromagnetism in (Ga,Mn)As. Instead, our data point to the existence of a Mn-derived impurity band even in samples with $x_{tot} \sim 6.8\%$; and, moreover, they show that it is the location of the Fermi level E_F within the impurity band, rather than the hole concentration itself, that determines T_C in (Ga,Mn)As. Specifically, samples with E_F located among localized states are insulating and show low T_C, whereas samples with the E_F located among the more extended states in the impurity band show high T_C and a metallic behaviour. Our results also indicate that, contrary to common belief[27,34–37], Mn_I are in fact necessary for achieving a high value of T_C, as predicted by Erwin and Petukhov[16]. Understanding their role is therefore crucial for guiding the growth and annealing conditions of (Ga,Mn)As.

The results of the channelling experiments and the corresponding values of T_C are presented in Table 1. The hole concentration p for a given sample in Table 1 was calculated as $p = 4(x_{sub} - 2x_I)/a^3$, where a is the lattice constant of (Ga,Mn)As in that sample calculated according to ref. 38. Although this is not a direct measurement of p, it provides an excellent estimate, as demonstrated by Wojtowicz *et al.*[35], who used electrochemical capacitance–voltage profiling in (Ga,Mn)As to measure p directly, and compared it with the values obtained from channelling experiments. We note parenthetically that, although arsenic antisites (As_{Ga}) also act as double donors in (Ga,Mn)As, their concentration is typically below $\sim 4 \times 10^{19}$ cm^{-3}, and their effect on p is therefore negligible in samples with $x_{tot} > 0.03$ (that is, for all the samples in this study)[39]. The value p/N_{Mn}^{eff} in the table represents the ratio of the hole concentration to the effective Mn concentration, a quantity relevant to the theoretical picture in ref. 33, which is also equal to the filling factor $f = (x_{sub} - 2x_I)/x_{eff}$ introduced later in this paper. Our data confirm the well-known fact[27,34] that a large fraction of Mn ions in the as-grown samples reside at interstitial sites. Specifically, the ratio x_I/x_{tot} is 6% for sample B; about 10% for samples C and D, and 25% for sample F. Sample F is rather striking in this respect: although it has the highest total Mn concentration, its x_{eff} is one of the lowest, and its p is the lowest of all samples because of the large value of x_I. Our data also confirm the well-known fact[11,30] that the main effect of annealing is the removal of Mn_I (presumably into random sites).

The first conclusion that can be drawn from Table 1 is that the data are in striking disagreement with the valence band model prediction that T_C increases monotonically with x_{eff} and p. For example, sample F* has the highest T_C of all samples, even though it has one of the lowest values of x_{eff} and of p. Moreover, sample D* has a T_C comparable to that of sample F, but the latter has the lowest of all p values and one of the lowest x_{eff}. A detailed comparison between our data and the prediction of the valence band model[33], which further illustrates these disagreements, is shown in Fig. 1.

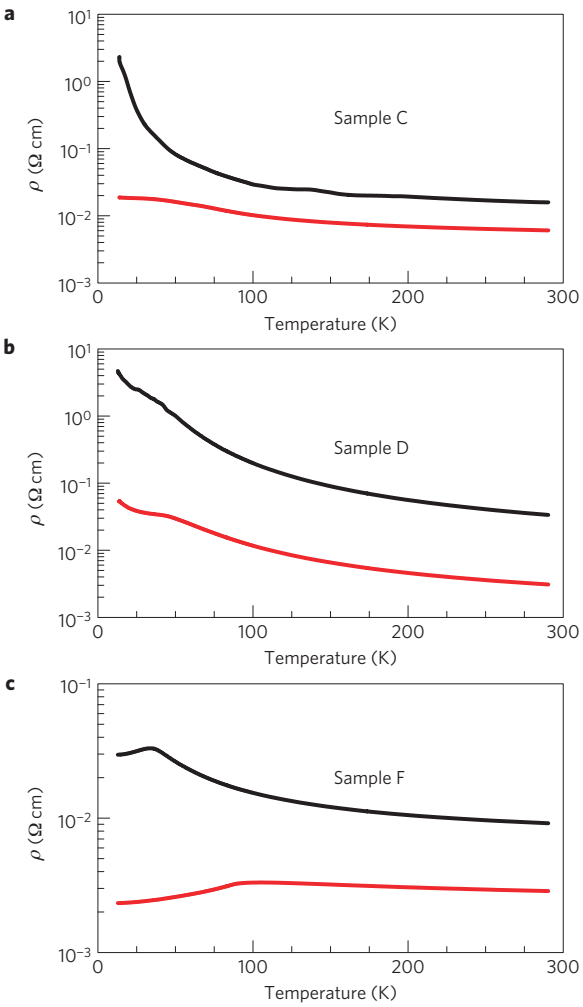

Figure 2 | Effect of annealing on transport properties of (Ga,Mn)As samples. The resistivity ρ was measured as a function of temperature for as-grown (black curves) and annealed (red curves) (Ga,Mn)As films: **a**, Samples C and C*, **b**, samples D and D*, and **c**, samples F and F*.

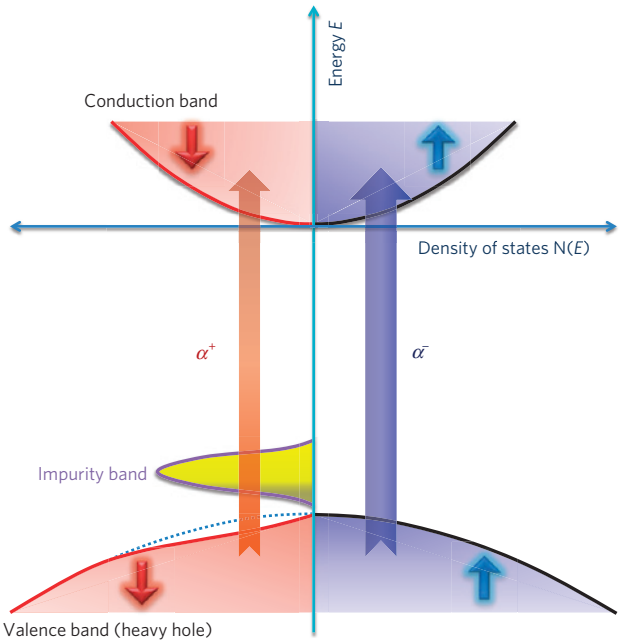

Figure 3 | Schematic representation of the origin of MCD in (Ga,Mn)As. Band structure of (Ga,Mn)As is shown for two spin orientations (not to scale; for more details see discussion in Supplementary Information). The creation of an impurity state near a substitutional Mn ion results in the depletion of the valence band by a state with spin oriented parallel to the Mn spin. When the impurity band is fully spin-polarized, there are fewer spin-down states than spin-up states left in the valence band. Consequently the absorption due to transitions from the valence band to the conduction band for the σ^+ circular polarization (marked α^+) is weaker than that for the opposite circular polarization (α^-), as indicated by the thickness of the long arrows. This spin-dependent difference in the DOS in the valence band leads then to a positive MCD signal that begins at the energy gap. As the DOS vanishes at the band-edges, this spin-dependent difference in the DOS will increase with energy, reaching a maximum where the spin-down DOS in the valence band is depleted the most by contributions to the impurity band, and again decreasing at higher energies. The light-hole band (not included in the figure for clarity) makes a similar contribution to MCD at higher energies.

The theory shown by the green line was compactly presented in ref. 33 as a plot of T_C/x_{eff} versus p/N_{Mn}^{eff}, the variable defined above, which can be seen as a measure of compensation level. (Low values of p/N_{Mn}^{eff} indicate samples with a high compensation level, and vice versa.) The red squares in the figure represent data from Table 1, and the blue squares are taken from ref. 40 for further comparison. For samples from ref. 40 the values of x_{eff} were found from channelling experiments as well, while p was taken from electrochemical capacitance–voltage profiling, a method that has been shown to agree very well with $x_{sub} - 2x_I$ (ref. 35). As can be seen from the figure, the experimental data show a highly non-monotonic behaviour, in sharp contrast to the valence band picture developed in ref. 33. Specifically, samples with a high degree of compensation are in agreement with the predictions of ref. 33; however, the lower the compensation level (that is, the larger the p/N_{Mn}^{eff} ratio), the more drastic is the disagreement between the valence band picture and our experiment. We emphasize that this disagreement has only come to light through the simultaneously obtained c-RBS and c-PIXE data, the strength of this approach being that both p and x_{eff} are determined by applying the same experimental method to each sample. It is especially important to note that, as the values of p and x_{eff} obtained by this method are directly related to each other, the uncertainty in the key parameter of the theory involved, that is, p/N_{Mn}^{eff}, is very small.

Further information is obtained from transport measurements. Figure 2 shows the resistivity ρ as a function of temperature T for samples C, D and F, both as-grown and annealed. All samples show lower resistivity on annealing, as expected, but interestingly the samples showing a clearly metallic behaviour (F and F*), have their hole concentrations among the lowest. In contrast, samples C, C*, D and D* show insulating behaviour (seen especially clearly for sample D), although all these samples have higher p than F and F*.

We now present the results of MCD measurements on the same set of samples. Earlier MCD studies on $Ga_{1-x}Mn_xAs$ with low Mn concentration ($x \approx 0.015$) revealed that the MCD signal originates from the spin-dependent difference in the density of states (DOS) in the valence band brought about by the presence of a Mn-derived spin-polarized impurity band, rather than from the p–d enhanced Zeeman splitting of the valence band[41]. This is consistent with recent findings that the p–d exchange splitting in the valence band is negligibly small[22,25]. The model developed earlier[41] is based on the fact that the creation of an impurity state near Mn_{Ga} results in a depletion of the valence band by a state with the spin oriented parallel to the Mn spin. Thus, when the impurity band is spin-polarized, fewer spin states parallel to the Mn spin are left in the valence band, as sketched in Fig. 3.

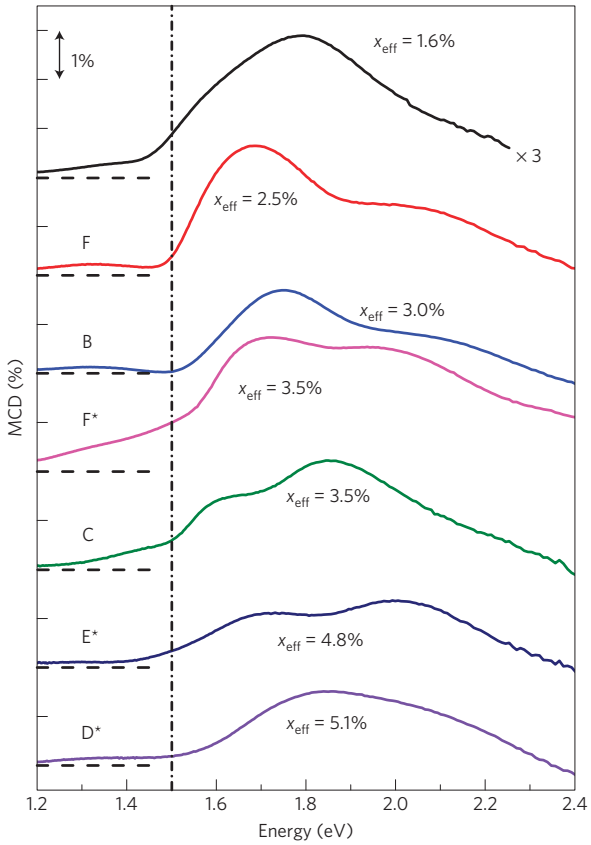

Figure 4 | MCD spectra. The spectra shown are taken at temperature $T = 10$ K and magnetic field $B = 5$ T. As the thickness of the layers is the same for all samples ($d \sim 100$ nm), the MCD signal $(T^+ - T^-)/(T^+ + T^-)$ expressed in % facilitates a good quantitative comparison between the samples. The vertical line shown at 1.5 eV indicates the bandgap of GaAs. The top spectrum, obtained for a sample with effective Mn concentration $x_{eff} = 1.6\%$, was published earlier[41], and is included here to show that the spectra obtained for samples with higher Mn concentrations evolve smoothly from low x_{eff} onward and show the same general features: a very broad positive signal that rises sharply at the bandgap. The peak which develops on the higher energy side and increases in intensity as x_{eff} increases reflects the increasing contribution to the impurity band from the light-hole band.

Figure 4 shows MCD spectra taken on six of the samples, in order of increasing x_{eff}. For comparison we also include MCD data for $x_{eff} = 0.016$ (ref. 41). All spectra show the same general features: a very broad positive signal that rises sharply at the energy gap (1.5 eV, indicated by the vertical line). Because the spectra for higher x_{eff} evolve smoothly, showing similar features as the spectra for $x_{eff} = 0.016$, we conclude that the model developed earlier[41] also applies to higher x_{eff}, that is, that MCD arises from a spin imbalance in the valence band states, a behaviour that can only be attributed to the existence of a spin-polarized impurity band. Furthermore, because the MCD signal rises sharply at the bandgap, not only must there be a difference in the spin-up and spin-down DOS at the top of the valence band, but these top valence band states must be occupied. Thus the Fermi level must lie above the top of the valence band, that is, in the impurity band.

As was also shown in ref. 41, in the case of very low Mn concentrations the largest contribution to impurity states comes from heavy holes. However, as the number of states in the impurity band increases with increasing x_{eff}, the light-hole states also begin to be pulled into the impurity band states. Figure 4 shows that as x_{eff} increases, a second peak begins to develop at higher energy

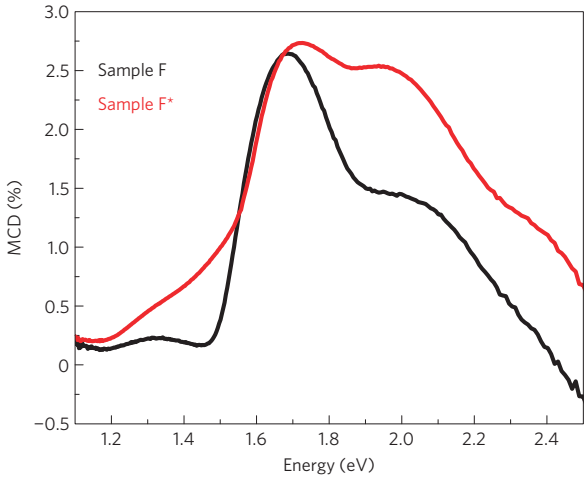

Figure 5 | Comparison between MCD spectra for samples F and F*. The spectra were taken at $T = 10$ K and magnetic field $B = 5$ T. The integrated intensity of the MCD signal for the annealed sample F* is significantly higher (~40%) than for the corresponding as-grown sample F. A below-gap negative contribution to the MCD signal is seen for sample F, as discussed in Supplementary Information.

with systematically increasing intensity. We therefore ascribe the two peaks observed in MCD to peak contributions from the heavy-hole band (lower energy peak) and from the light-hole band (higher energy peak).

Although the existence of an impurity band for $x_{tot} \sim 0.068$ is sometimes questioned, we argue that it is actually x_{eff} that controls the number of impurity states. The experimental evidence for this comes from Fig. 4, which reveals that samples with similar x_{eff} exhibit similar MCD spectra. Especially striking is the resemblance between the spectra for samples F and B, even though they have very different values of x_{tot}, p, and T_C (see Table 1). The only property which these samples have in common is their small x_{eff}. This behaviour, together with the evolution of the light-hole peak in the MCD spectra with increasing x_{eff}, provides a clue that it is x_{eff} rather than x_{tot}, or even x_{sub}, that controls the shape of MCD spectra.

Further confirmation that x_{eff} controls the number of impurity states is presented in Fig. 5, where we compare the MCD spectra for samples F and F*. As shown in Table 1, both samples have very similar values of x_{sub}. However, x_{eff} increases from 2.5% in F to 3.5% in F*. As the MCD signal arises from the spin-dependent difference in the DOS in the valence band, and because the number of spin-up states missing from the valence band must equal the number of states of the same spin in the impurity band, the integrated MCD signal over the energy range above the bandgap must reflect the number of states in the impurity band . The increase of the MCD signal in the annealed sample F* in Fig. 5 thus indicates that the number of states in the impurity band is determined by x_{eff}. Other samples also show some increase in the integrated MCD on annealing, but because annealing in those samples leads only to small increases of x_{eff}, the effect is not as marked as in F and F*.

We now discuss these findings in the context of the unsolved issue concerning the states occupied by the holes mediating the Mn–Mn ferromagnetic coupling. As already mentioned, our results disagree with the models based on the valence band picture. Furthermore, the MCD data for nominal Mn concentrations of up to ~6.8% are consistent with the model predicting that MCD arises from the spin imbalance in the valence band originating from the presence of a spin-polarized impurity band, and that E_F lies above the top of the valence band in all our samples. As the data also show that the number of states in the impurity band is determined by x_{eff},

the hole fraction p/N_{Mn}^{eff} listed in Table 1 is recognized as the filling factor f of the impurity band, $f=(x_{sub}-2x_I)/x_{eff}$, and thus gives the location of the Fermi level within the impurity band. For example, $f=0.75$ indicates that 25% of the impurity band states are occupied by electrons, whereas $f=0.9$ indicates that only 10% of the impurity band states are occupied by electrons, putting the Fermi level near the bottom of the impurity band.

Taking all our data together, we argue that the behaviour of the Curie temperature of (Ga,Mn)As can be understood only by assuming that its ferromagnetism is mediated by holes residing in the impurity band, and that it is the location of the Fermi level within the impurity band that determines T_C. We can now re-examine Fig. 1 and see how T_C/x_{eff} changes as the Fermi level moves from the top of the impurity band ($f\approx0.2$) to the bottom ($f\approx0.9$). As the figure shows, samples with $f\approx0.7$ have the highest T_C/x_{eff} ratio, and that ratio drops for lower as well as for higher values of f. This 'dome-like' behaviour of T_C/x_{eff} versus f agrees conceptually with the prediction that T_C is expected to be highest at $f\approx0.5$ in the impurity band, because ferromagnetic alignment is promoted by hole hopping, which is only possible between singly occupied and empty Mn impurity states[16]. This result is also in agreement with the simulations of ref. 42, which find extended states and the highest DOS close to the centre of the impurity band, meaning that the most metallic samples with the highest T_C have their Fermi level in this region. In contrast, for small or large f, that is, when the Fermi level is near the top or the bottom of the impurity band, the DOS is lower and the states become localized, suggesting insulating samples with lower T_C. As an illustration, samples A and F* have their Fermi levels close to the centre of the impurity band; thus they have the highest T_C/x_{eff} ratio, and are also most metallic. However, more detailed theoretical modelling is needed before quantitative comparisons can be undertaken.

Comparing samples with similar filling factors of $f\sim0.9$ also provides a valuable insight into the effect of annealing. As shown in Fig. 2, the resistivities in annealed samples, especially C* and D*, decrease by about two orders of magnitude after annealing. Because f also increases slightly, thus moving E_F towards more localized states, we are forced to conclude that annealing lowers the disorder and improves the uniformity of the sample. As a consequence, the energy range where the states are extended is expanded, resulting in an increased T_C. This agrees with neutron reflection measurements[43] and ferromagnetic resonance experiments[44] which also show that one of the major effects of annealing is to improve the homogeneity of (Ga,Mn)As samples.

In summary, our data are consistent with the existence of an impurity band up to rather high nominal Mn doping levels, and indicate that the location of the Fermi level within the impurity band plays a crucial role in determining T_C through determining the degree of localization of the impurity band holes. Specifically, we show that having the Fermi level near the middle of the impurity band, where the states are most extended, is at least as important for raising T_C as increases in x_{eff}. An understanding of the role of E_F thus opens pathways for new strategies for achieving higher values of T_C. For example, appropriate control of the concentration of Mn_I, co-doping with donor ions[40], or modulation doping can be used to engineer the location of E_F within the impurity band to best advantage. Similarly, the findings of this paper have far-reaching consequences for optimizing the ferromagnetic coupling (and therefore T_C) within the whole family of III-Mn-V ferromagnetic semiconductors through tuning the binding energy of the Mn acceptors by means of, for example, alloying different III–V host materials. By varying the binding energy of Mn acceptors one can vary the location and the width of the impurity band, and therefore improve the Curie temperature through improving the mobility of the impurity band holes.

Methods

Synthesis of (Ga,Mn)As samples. (Ga,Mn)As samples with a thickness of ~100 nm were grown by low-temperature molecular beam epitaxy (LT-MBE) on (001) GaAs substrates on which a 0.2 μm $Ga_{0.70}Al_{0.30}As$ buffer was first deposited. The annealed samples were treated at 280 °C for 1 h in flowing N_2 gas. Superconducting quantum interference device (SQUID) magnetometry was used to measure the magnetization of the samples as a function of temperature and thus determine T_C. These measurements were complemented by electrical transport characterization as a function of temperature.

Magneto-optical spectroscopy. The MCD measures the difference in absorption of right- and left- circularly polarized light, and is given by the expression

$$\mathrm{MCD}=\frac{T^+-T^-}{T^++T^-}\sim\frac{(\alpha^--\alpha^+)d}{2}$$

where T^+ and T^- are transmission intensities for σ^+ and σ^- circular polarizations, $\alpha\pm$ are the corresponding absorption coefficients, and d is the thickness of the sample. As the MCD measurements were performed in a transmission mode, the GaAs substrate had to be removed through polishing and subsequent etching, the $Ga_{0.70}Al_{0.30}As$ buffer serving as an excellent etch stop. The measurements of MCD were carried out by means of the polarization modulation produced by a photo-elastic modulator. The samples were placed in an optical cryostat equipped with a 6 Tesla superconducting magnet, and the magnetic field was applied parallel to the direction of light propagation, that is, normal to the (Ga,Mn)As layers. The transmitted light was detected by a photodiode using a lock-in amplifier.

Channelling experiment. The total Mn concentration and the locations of Mn sites in the $Ga_{1-x}Mn_xAs$ lattice were studied by simultaneous c-RBS and c-PIXE measurements using a 1.95 MeV $^4He^{++}$ beam. Backscattered He ions and characteristic X-rays excited by the He ions were detected by a Si surface barrier detector located at a backscattering angle of 165° and a Si(Li) detector located at 30° with respect to the incident ion beam. The specific locations of Mn atoms in the lattice were determined by directly comparing the angular scans about the ⟨110⟩ and ⟨111⟩ axial channels of the Mn Kα X-ray signals (PIXE) with those of the RBS signals from the GaAs host lattice. The accuracy of determining the quantities x_{sub}, x_I and x_{tot} relevant to the present paper is estimated as ±10%.

Received 24 August 2011; accepted 18 January 2012; published online 19 February 2012

References

1. Dietl, T. A ten-year perspective on dilute magnetic semiconductors and oxides. *Nature Mater.* **9,** 965–974 (2010).
2. Dietl, T., Ohno, H., Matsukura, F., Cibert, J. & Ferrand, D. Zener model description of ferromagnetism in zinc-blende magnetic semiconductors. *Science* **287,** 1019–1022 (2000).
3. Jungwirth, T. *et al.* Character of states near the Fermi level in (Ga,Mn)As: Impurity to valence band crossover. *Phys. Rev. B* **76,** 125206 (2007).
4. Sawicki, M. Magnetic properties of (Ga,Mn)As. *J. Magn. Magn. Mater.* **300,** 1–6 (2006).
5. Neumaier, D. *et al.* All-electrical measurements of the density of states in (Ga,Mn)As. *Phys. Rev. Lett.* **103,** 087203 (2009).
6. Sawicki, M. *et al.* Experimental probing of the interplay between ferromagnetism and localization in (Ga,Mn)As. *Nature Phys.* **6,** 22–25 (2010).
7. Richardella, A. *et al.* Visualizing critical correlations near the metal–insulator transition in $Ga_{1-x}Mn_xAs$. *Science* **327,** 665–669 (2010).
8. Boukari, H. *et al.* Light and electric field control of ferromagnetism in magnetic quantum structures. *Phys. Rev. Lett.* **88,** 207204 (2002).
9. Jungwirth, T., König, J., Sinova, J., Kučera, J. & MacDonald, A. H. Curie temperature trends in (III, Mn)V ferromagnetic semiconductors. *Phys. Rev. B* **66,** 012402 (2002).
10. Nishitani, Y. *et al.* Curie temperature versus hole concentration in field-effect structures of $Ga_{1-x}Mn_xAs$. *Phys. Rev. B* **81,** 045208 (2010).
11. Wang, K. Y. *et al.* Influence of the Mn interstitial on the magnetic and transport properties of (Ga,Mn)As. *J. Appl. Phys.* **95,** 6512–6514 (2004).
12. Ku, K. C. *et al.* Highly enhanced Curie temperature in low-temperature annealed [Ga,Mn]As epilayers. *Appl. Phys. Lett.* **82,** 2302–2304 (2003).
13. Sato, K., Dederichs, P. H. & Katayama-Yoshida, H. Curie temperatures of III–V diluted magnetic semiconductors calculated from first principles. *Europhys. Lett.* **61,** 403–408 (2003).
14. Berciu, M. & Bhatt, R. N. Effects of disorder on ferromagnetism in diluted magnetic semiconductors. *Phys. Rev. Lett.* **87,** 107203 (2001).
15. Mahadevan, P. & Zunger, A. Trends in ferromagnetism, hole localization, and acceptor level depth for Mn substitution in GaN, GaP, GaAs, GaSb. *Appl. Phys. Lett.* **85,** 2860–2862 (2004).
16. Erwin, S. C. & Petukhov, A. G. Self-compensation in Manganese-doped ferromagnetic semiconductors. *Phys. Rev. Lett.* **89,** 227201 (2002).

17. Alberi, K. *et al.* Formation of Mn-derived impurity band in III-Mn-V alloys by valence band anticrossing. *Phys. Rev. B* **78,** 075201 (2008).
18. Mayer, M. A. *et al.* Electronic structure of $Ga_{1-x}Mn_xAs$ analyzed according to hole-concentration-dependent measurements. *Phys. Rev. B* **81,** 045205 (2010).
19. Burch, K., Awschalom, D. & Basov, D. Optical properties of III-Mn-V ferromagnetic semiconductors. *J. Magn. Magn. Mater.* **320,** 3207–3228 (2008).
20. Burch, K. S. *et al.* Impurity band conduction in a high temperature ferromagnetic semiconductor. *Phys. Rev. Lett.* **97,** 087208 (2006).
21. Rokhinson, L. P. *et al.* Weal localization in $Ga_{1-x}Mn_xAs$: Evidence of impurity band transport. *Phys. Rev. B* **76,** 161201 (2007).
22. Ohya, S., Muneta, I., Hai, P. N. & Tanaka, M. Valence-band structure of the ferromagnetic semiconductor (Ga,Mn)As studied by spin-dependent resonant tunneling spectroscopy. *Phys. Rev. Lett.* **104,** 167204 (2010).
23. Sheu, B. L. *et al.* Onset of ferromagnetism in low-doped $Ga_{1-x}Mn_xAs$. *Phys. Rev. Lett.* **99,** 227205 (2007).
24. Tang, J-M. & Flatte, M. E. Magnetic circular dichroism from the impurity band in III–V diluted magnetic semiconductors. *Phys. Rev. Lett.* **101,** 157203 (2008).
25. Ohya, S., Takata, K. & Tanaka, M. Nearly non-magnetic valence band of the ferromagnetic semiconductor (Ga,Mn)As. *Nature Phys.* **7,** 342–347 (2011).
26. Chapler, B. C. *et al.* Infrared probe of the insulator-to-metal transition in $Ga_{1-x}Mn_xAs$ and $Ga_{1-x}Be_xAs$. *Phys. Rev. B* **84,** 081203 (2011).
27. Yu, K. M. *et al.* Effect of the location of Mn sites in ferromagnetic $Ga_{1-x}Mn_xAs$ on its Curie temperature. *Phys. Rev. B* **65,** 201303 (2002).
28. Blinowski, J. & Kacman, P. Spin interactions of interstitial Mn ions in ferromagnetic (Ga,Mn)As. *Phys. Rev. B* **67,** 121204 (2003).
29. Mašek, C. J. & Máca, F. Interstitial Mn in (Ga,Mn)As: Binding energy and exchange coupling. *Phys. Rev. B* **69,** 165212 (2004).
30. Edmonds, K. W. *et al.* Mn Interstitial Diffusion in (Ga,Mn)As. *Phys. Rev. Lett.* **92,** 037201 (2004).
31. Bouzerar, G., Ziman, T. & Kudrnovský, J. Compensation, interstitial defects, and ferromagnetism in diluted ferromagnetic semiconductors. *Phys. Rev. B* **72,** 125207 (2005).
32. Takeda, Y. *et al.* Nature of magnetic coupling between Mn ions in As-Grown $Ga_{1-x}Mn_xAs$ studied by X-Ray magnetic circular dichroism. *Phys. Rev. Lett.* **100,** 247202 (2008).
33. Jungwirth, T. *et al.* Prospects for high temperature ferromagnetism in (Ga,Mn)As semiconductors. *Phys. Rev. B* **72,** 165204 (2005).
34. Yu, K. M. *et al.* Curie temperature limit in ferromagnetic $Ga_{1-x}Mn_xAs$. *Phys. Rev. B* **68,** 041308 (2003).
35. Wojtowicz, T., Furdyna, J. K., Liu, X., Yu, K. M. & Walukiewicz, W. Electronic effects determining the formation of ferromagnetic $III_{1-x}Mn_xV$ alloys during epitaxial growth. *Physica E* **25,** 171–180 (2004).
36. MacDonald, A. H., Schiffer, P. & Samarth, N. Ferromagnetic semiconductors: Moving beyond (Ga,Mn)As. *Nature Mater.* **4,** 195–202 (2005).
37. Yu, K. M. *et al.* in *Fermi Level Effects on Mn Incorporation in III-Mn-V Ferromagnetic Semiconductors* Vol. 82 (eds Dietl, T., Awchalom, D. D., Kamińska, M. & Ohno, H.) (Spintronics, Semiconductors and Semimetals, Elsevier, 2008).
38. Sadowski, J. *et al.* Structural and magnetic properties of (Ga,Mn)As layers with high Mn-content grown by migration-enhanced epitaxy on GaAs(100) substrates. *Appl. Phys. Lett.* **78,** 3271–3273 (2001).
39. Wolos, A. *et al.* Properties of arsenic antisite defects in $Ga_{1-x}Mn_xAs$. *J. Appl. Phys.* **96,** 530–533 (2004).
40. Cho, Y. J., Yu, K. M., Liu, X., Walukiewicz, W. & Furdyna, J. K. Effects of donor doping on $Ga_{1-x}Mn_xAs$. *Appl. Phys. Lett.* **93,** 262505 (2008).
41. Berciu, M. *et al.* Origin of magnetic circular dichroism in (Ga,Mn)As: Giant Zeeman splitting vs. spin dependent density of states. *Phys. Rev. Lett.* **102,** 247202 (2009).
42. Moca, C. P., Zarand, G. & Berciu, M. Theory of optical conductivity for dilute $Ga_{1-x}Mn_xAs$. *Phys. Rev. B* **80,** 165202 (2009).
43. Kirby, B. J. *et al.* Annealing-dependent magnetic depth profile in $Ga_{1-x}Mn_xAs$. *Phys. Rev. B* **69,** 081307 (2004).
44. Liu, X., Sasaki, Y. & Furdyna, J. K. Ferromagnetic resonance in $Ga_{1-x}Mn_xAs$. *Phys. Rev. B* **67,** 205204 (2003).

Acknowledgements

K.T. thanks Y-Y. Zhou for her help with the MCD set-up and sample preparation. This work was supported by the National Science Foundation Grant DMR 10-05851; by the Natural Sciences and Engineering Research Council of Canada (NSERC) and the Canadian Institute for Advanced Research (CIFAR) and by the Director, Office of Science, Office of Basic Energy Sciences, Materials Sciences and Engineering Division, of the US Department of Energy under Contract No. DE — AC02-05CH11231.

Author contributions

M.D. and M.B. conceived the project and wrote the manuscript. K.T. carried out the MCD, transport and magnetization experiments with guidance from X.L., M.D. and J.K.F. X.L. fabricated the samples and contributed to the manuscript. K.M.Y. and W.W. are responsible for the channelling experiments. The project was supervised by M.D. and J.K.F. All authors have reviewed, discussed and approved the results and conclusions of this article.

Additional information

The authors declare no competing financial interests. Supplementary information accompanies this paper on www.nature.com/naturematerials. Reprints and permissions information is available online at www.nature.com/reprints. Correspondence and requests for materials should be addressed to M.D.